Wu *et al. Cell Communication and Signaling* (2024) 22:409
https://doi.org/10.1186/s12964-024-01784-7

Cell Communication and Signaling

RESEARCH Open Access

Terphenyllin induces CASP3-dependent apoptosis and pyroptosis in A375 cells through upregulation of p53

Wei Wu[1], Meng-Yuan Wu[1], Ting Dai[1], Li-Na Ke[1], Yan Shi[1], Jin Hu[1*] and Qin Wang[1*]

Abstract

Background Melanoma, one of the most lethal forms of skin cancer, has the potential to develop in any area where melanocytes are present. Currently, postoperative recurrence due to the emergence of systemic drug resistance represents a significant challenge in the treatment of melanoma. In this study, terphenyllin (TER), a distinctive inhibitory impact on melanoma cells was identified from the natural p-terphenyl metabolite. This study aimed to elucidate the intrinsic mechanism of this inhibitory effect, which may facilitate the discovery of novel chemotherapeutic agents.

Methods A transcriptome sequencing and metabolomic analysis of TER-treated A375 cells was conducted to identify potential pathways of action. The key proteins were knocked out and backfilled using CRISPR-Cas9 technology and molecular cloning. Subsequently, the results of cytosolic viability, LDH release, immunofluorescence and flow cytometry were employed to demonstrate the cell death status of the drug-treated cells.

Results The p53 signalling pathway was markedly upregulated following TER treatment, leading to the activation of CASP3 via the intrinsic apoptotic pathway. The activated CASP3 initiated apoptosis, while simultaneously continuing to cleave the GSDME, thereby triggering pyroptosis. The knockout of p53, a key protein situated upstream of this pathway, resulted in a significant rescue of TER-induced cell death, as well as an alleviation of the decrease in cell viability. However, the knockout of key proteins situated downstream of the pathway (CASP3 and GSDME) did not result in a rescue of TER-induced cell death, but rather a transformation of the cells from apoptosis and pyroptosis.

Conclusions The induction of apoptosis and pyroptosis in A375 cells by TER is mediated via the p53-BAX/FAS-CASP3-GSDME signalling pathway. This lays the foundation for TER as a potential anti-melanoma drug in the future. It should be noted that CASP3 and GSDME in this pathway solely regulate the mode of cell death, rather than determine whether cell death occurs. This distinction may prove valuable in future studies of apoptosis and pyroptosis.

Keywords Terphenyllin, Melanoma, Apoptosis, CASP3, GSDME

*Correspondence:
Jin Hu
jinhu@xmu.edu.cn
Qin Wang
qwang@xmu.edu.cn
[1]State Key Laboratory of Cellular Stress Biology, School of Life Sciences, Xiamen University, Xiamen, PR China

Introduction

Melanomas originate from melanocytes, which are a type of neural crest-derived cell. During the process of development, these cells disseminate to various locations within the body, including the skin, eyes, and other tissues [1]. Melanoma has become a rapidly growing cancer type in developed countries. In the United States, the incidence of melanoma increased from 7.9/100 000 in 1975 to 25.3/100 000 in 2018, representing a more than 320% increase. Similarly, in the UK, the incidence of melanoma increased from 5.8 to 19.8 between 1982 and 2011, and in Sweden and Australia, it increased from 13.0 to 28.3 and from 26.4 to 51.6, respectively [2]. Globally, approximately 232 100 (1.7%) newly diagnosed cases of primary cutaneous melanoma (excluding non-melanoma skin cancers) occur each year, resulting in approximately 55 500 cancer-related deaths (0.7% of all cancer deaths) [3]. In the United States, the incidence rate is at least 16 times greater among Caucasians than among African Americans and 10 times greater than among Hispanics [4].

At present, surgical resection, chemotherapy, targeted therapy and immunotherapy represent the primary modalities of treatment for melanoma [5]. Surgical resection of the tumor and surrounding healthy tissue is the main treatment for localized melanoma [6]. However, in patients with metastatic melanoma, surgical treatment alone is not curative and medication is also required [7]. In recent years, immune checkpoint blockade (ICB) therapy has achieved great success in clinical studies of advanced melanoma, with objective remission rates of 19%, 45%, and 58% for anti-CTLA4, anti-PD1, and anti-CTLA4 and anti-PD1 combination therapy, respectively [8]. While ICB has been demonstrated to improve the prognosis of patients with metastatic melanoma, it is important to note that not all patients will benefit from this treatment [9]. A subset of patients who initially responded to immunotherapy subsequently exhibited relapse and developed acquired resistance, while others demonstrated no response at all [10]. BRAF-targeted and MEK-targeted therapies are also available for adjuvant use in the 40% of patients with BRAFV600-mutant melanoma [7]. Three combinations (dabrafenib plus trametinib, vemurafenib plus cobimetinib, and encorafenib plus binimetinib) have been observed to elicit a high initial response rate, with evidence of tumour regression in nearly all patients [11–13]. Despite the initial efficacy of targeted therapies, the emergence of resistance appears to be a common issue associated with these drugs [14–16]. Therefore, further mechanistic exploration of potential new drugs remains of great importance.

P-terphenyl metabolites are commonly found in macrofungi and are polyaromatic derivatives [17]. Some p-terphenyls, particularly those with 4,2′,4″-trihydroxy or 4,4″-dihydroxy-1,2,1′,2′-furan substituent nuclei, exhibit significant antioxidant and α-glucosidase inhibitory activities [18]. Terphenyllin (TER), a natural p-terphenyl compound derived from the fungus *Aspergillus candidus*, has been shown to inhibit α-glucosidase activity and cytotoxicity [19]. Recent studies have also reported its inhibitory effects on pancreatic tumors and gastric cancers [20, 21]. In this study, we focused on the melanoma cell line A375 and investigated the type of cell death induced by TER treatment, as well as its specific mechanism of action, through transcriptome sequencing and metabolome analysis.

Materials and methods

Cell culture

The Human A375, M14 and QBC939 cells were stored in the laboratory of School of Life Sciences, Xiamen University. HepG2, UmUc3, Hela and HaCat cells were obtained from Procell Life Science and Technology (Wuhan, China). All cells were mycoplasma negative as routinely demonstrated by PCR using the Mycoplasma PCR Detection Kit (C0301S#, Beyotime, Shanghai, China), and cultured in DMEM (12800-017#, Gibco, Carlsbad, CA, USA) supplemented with 10% FBS (AB-FBS0500#, ABW, Shanghai, China). When the cells reached 70% confluence, they were treated with either TER (Terphenyllin, HY-119821#, MCE, NJ, USA) or cisplatin for 48 h. Alternatively, they were incubated in the presence or absence of cell death inhibitor inhibitors, which included cellular autophagy inhibitors: wortmannin (100 nM, MCE, NJ, USA), chloroquine (20 μM, MCE, NJ, USA); apoptosis pathway inhibitor: z-VAD-fmk (20 μM, Beyotime, Shanghai, China); antioxidants: Butylated hydroxyanisole (BHA, 100 μM, MCE, NJ, USA), Necrostatin-1 (30 μM, Beyotime, Shanghai, China); iron death inhibitor: Ferrostatin-1 (0.5μM, MCE, NJ, USA); caspase-1 specific inhibitor: VX-765 (50 μM, MCE, NJ, USA). A375 cells were pretreated with these inhibitors for 2 h, and then each pretreatment group was co-treated with TER for 48 h. The cells were then incubated in DMEM at 37 °C with 5% CO_2.

Cell viability assay

For the cell viability assay, 10,000 cells were seeded into 96-well plates and incubated overnight with the indicated experimental treatments. At the specified time points, 10 μL of freshly prepared MTT solution (5%, T31640#, Acmec, Shanghai, China) was added to each well (containing 100 μL of cell culture medium) and incubated at 37 °C for 3 h. The absorbance was determined using a full-wavelength microplate reader (Thermo Fisher Scientific Oy Ratastise 2, FI-01620 Vantaa, Finland) at a wavelength of 490 nm.

$$\text{Cell viability}\,(\%) = (A_{\text{sample}} - A_{\text{blank}}) / (A_{\text{control}} - A_{\text{blank}}) \times 100\%$$

For crystal violet staining, cells were inoculated into a 6-well plate and placed in a humidity-saturated, 5% CO2, 37 °C cell culture incubator. Once the A375 cells had adhered to the wall, they were treated with varying concentrations of TER for a period of 48 h. The treated cells were then fixed with 4% paraformaldehyde for 20 min, after which they were stained with a 0.1% crystal violet solution for a further 30 min. Imaging was conducted and documented.

LDH release test

The LDH levels were quantified using an LDH Cytotoxicity Assay Kit (C0017#, Beyotime, Shanghai, China) in accordance with the manufacturer's instructions. Subsequently, the absorbance at 490 nm was measured. Each experiment was repeated four times.

$$\text{LDH activity (relative fold change)} = (OD_{\text{sample}}/OD_{\text{control}}) \times 100\%$$

Cell colony formation assay

A375 cells were plated in 6-well plates (1000 cells/well) and then incubated at 37 °C in 5% CO_2 until the cells completely adhered to the walls of the plates. The cell culture medium was replaced with medium containing different concentrations of TER for a 48-hour incubation period. Subsequently, the medium containing TER was discarded, and the cells were allowed to culture in new media for 10 days. Then, the cells were fixed with anhydrous ethanol at room temperature for 15 min and washed twice with PBS. The cells were then stained with Giemsa at room temperature for 15 min, washed with PBS twice and photographed. Finally, the colonies were manually counted and recorded.

Transwell cell invasion assay

Cells were treated with different doses of TER for 48 h, treated cells were digested and prepared into cell suspension and adjusted to the same concentration. Configure the matrix gel by referring to the instructions of Biozellen® 3D Cell Culture Matrix Gel Kit (B-P-00003-4#, Biozellen, NE, USA). After the matrix gel had completely solidified, 0.1 mL of serum-free, cell density 5×10^4 cells/well cell suspension was added to the upper chamber of the Transwell (3422#, Corning, NY, USA). Add 0.8 mL of complete culture medium to the lower chamber of the Transwell as a chemoattractant. A375 cells that still retain the ability to migrate and invade or have a strong ability to migrate and invade can migrate and invade from the upper layer of the cell chamber by secreting matrix protease to the lower membrane of the cell chamber. The cells were incubated at 37°C for 24 h and fixed in 75% ethanol at room temperature for 15 min. Fixed cells were stained with Giemsa stain for 10 min, dried, and the invasion was recorded using an inverted phase contrast microscope.

Assessment of apoptosis and the cell cycle distribution by flow cytometry

Cells were treated with different doses of TER for 24 h, 30 h, or 48 h for flow cytometry detection. The cells were collected by trypsinization and washed twice with phosphate-based buffer. Then, the cells were labeled using an Annexin V-FITC/PI Apoptosis Detection Kit (C1062M#, Beyotime, Shanghai, China) according to the manufacturer's protocol. Apoptosis was assessed via flow cytometry (Quanteon, ACEA Biosciences, CA, USA).

For the cell cycle assay, 5 μL of PI staining solution was added to the cells protected from light after they were collected by trypsinization and washed with PBS. The cells were filtered through a 300mesh sieve in an ice bath for 0.5 h and analyzed using a flow cytometer (Beckman FC500, CA, USA) with 10,000 events for each group of cells. The obtained results were analyzed using ModFit software (ModFit LT v3.2) to generate a cell cycle analog graph and calculate the percentage of cells in each phase.

Immunofluorescence and confocal microscopy

A375 cells were seeded on coverslips at 30% confluence in six-well culture dishes. The cells were transfected with the appropriate constructs and incubated for an additional 24 h. Next, the cells were washed three times with PBS and fixed with 4% (v/v) paraformaldehyde for 15 min at room temperature. The fixed cells were then washed with PBS and incubated with 0.2% Triton X-100 and 0.2% BSA in PBS for 10 min on ice for permeabilization. After permeabilization, nonspecific binding was blocked by incubation with 0.02% Triton X-100 and 5% BSA in PBS for 30 min at room temperature. The cells were then incubated with specific primary antibodies (listed in Table S1) for 1 h. After three washes with PBS, the cells were incubated with secondary antibodies (Alexa Fluor 488-coupled anti-mouse IgG (AS057#, ABclone, Wuhan, China) and Alexa Fluor 555-coupled anti-rabbit IgG (AS053#, ABclone, Wuhan, China)) for 1 h, followed by incubation with DAPI solution (C0065#, Solarbio, Beijing, China) for 20 min. Finally, the cells were washed with PBS three times and blocked with glycerol. Confocal images were obtained using a confocal microscope (Leica TCS SP8 DLS, Hessian, Germany).

Microscopic imaging

Cells were seeded in 6-well plates and stained in situ according to the instructions of the Annexin V-FITC/PI

Apoptosis Detection Kit (C1062M#, Beyotime, Shanghai, China). Both static bright-field images and fluorescence images were captured using an Olympus microscope (OLYMPUS IX51, Tokyo, Japan).

CRISPR-Cas9 knockout

The generation of knockout (KO) cell lines using CRISPR-Cas9 technology was performed according to the literature [22]. The sgRNA sequences for *TP53*, *CASP3*, and *GSDME* were designed using the online guide https://www.vbc-score.org/. The specific sgRNA sequences used were as follows: p53-sg2 5'-CAAGCAG TCACAGCACATG-3', CASP3-sg4 5′-GTGAGCATGG AAACAATACA-3′, GSDME-sg1 5′- TGTCACCAAGG ACTCCAACG-3′. To construct the px458-p53/CASP3/GSDME-KO plasmid, the pSpCas9(BB)-2 A-Puro plasmid (62988#, PX459, Addgene) was digested and ligated with the annealed sgRNA through the Bbs1 (R0539S#, NEB, MA, USA) restriction site. A375 cells in 6-well plates were transfected with 2 μg/well of the px458-p53/CASP3/GSDME-KO plasmid using polyethyleneimine (9002-98-6#, Acmec, Shanghai, China). After 48 h, Puro (HY-K1057#, MCE, NJ, USA) was added to the culture medium. The Puro-containing medium was changed every 2–3 days, and the control cells were replaced with fresh medium immediately after complete cell death was observed. Once the cells reached 70% confluence, individual cells were selected by limited dilution and seeded in 96-well plates. After 2–3 weeks, each single clone was detected by protein blotting to confirm the knockout efficiency.

Recombinant plasmid construction

Total RNA was isolated from A375 cells using TRIzol reagent (R401-01#, Vazyme, Nanjing, China). cDNA was synthesized with a PrimeScript RT Reagent Kit (RR047A#, Takara, Kyoto, Japan). The coding sequence of the target gene was amplified from the human cDNA library by PCR using a primer set (Table S2). The amplicon was cloned and inserted into the pCMV vector through ligation–independent cloning. The constructed plasmids were verified by sequencing and then transfected into 12-well plates using polyethyleneimine (PEI) at a concentration of 1 μg per well.

Real-time fluorescence quantitative PCR

Total cellular RNA was extracted using the TRIzol reagent and subsequently reverse transcribed into cDNA. Quantitative qRT−PCR was conducted using the CFX384 Touch system (Bio-Rad, CA, USA) and the Genious 2x SYBR Green kit (RM21204#, ABclone, Wuhan, China). The primers used for qRT−PCR were validated and obtained from Sangon Biotech (Sangon Biotech, Shanghai, China), as shown in Table S3. GAPDH or ACTIN was utilized as a control gene for normalization purposes.

SDS–PAGE and western blot analysis

Cells were seeded in 12-well plates and allowed to adhere overnight. The cells were then treated with TER as indicated or transfected with the appropriate constructs for 24 h and harvested in 2× loading buffer. Proteins were separated by SDS−PAGE and transferred to PVDF membranes (Millipore, MA, USA). The membrane was blocked in 5% BSA for one hour and then incubated with the target primary antibody (Table S1) overnight. Following incubation, the membrane was washed three times with 1× TBST and then incubated with secondary antibodies (rabbit or mouse, AS014#, anti-Rabbit IgG; anti-Mouse IgG, ABclone, Wuhan, China) conjugated with horseradish peroxidase (HRP) for 2 h at room temperature. After the membrane was washed three times, the results were imaged using a gel image analysis system (Azure Biosystems C280, CA, USA) according to the manufacturer's instructions.

Transcriptome analysis

Purified total RNA was extracted from A375 cells treated for different durations using TRIzol reagent. These RNA samples were subsequently sent to a transcriptome sequencing company, Novogene (Beijing, China), for RNA-Seq analysis. The analysis was performed using an Illumina HiSeq 4000 system. For quantification of gene expression, the fragments per kilobase of transcript per million fragments mapped (FPKM) method was used. To identify differentially expressed genes (DEGs), criteria were established for genes with a log2 (fold change)>1 and Q<0.001 to be considered DEGs. Heatmaps of gene expression, GO (gene ontology) enrichment analyses and enriched KEGG (Kyoto Encyclopedia of Genes and Genomes) pathway analyses were generated based on the DEGs.

Metabolomic analysis

The metabolite analysis involved liquid chromatography using a SCIEX ExionLC AD and a Millipore ZIC-pHILIC column for separation (5 μm, 2.1×100 mm internal dimensions, PN: 1.50462.0001). The column was maintained at 40 °C, and each sample was injected with a volume of 2 μL. The mobile phase, consisting of 15 mM ammonium acetate and 3 mL/L ammonium hydroxide in LC−MS grade water, as well as LC−MS grade 90% acetonitrile–HPLC water, was run at a flow rate of 0.2 mL/min. The compounds were separated using a gradient program, starting with 95% B for 2 min, decreasing to 45% B in 13 min, holding for 3 min, and setting a post time of 4 min. A QTRAP 5500 mass spectrometer was used to

measure metabolites in a gas mixture. The data were then analyzed using MultiQuant Software (AB SCIEX).

Statistical analysis

Each experiment was repeated three or four times. The data are presented as the SDs±means, and Student's t test or one-way ANOVA with Dunnett correction to account for multiple comparisons. All the statistical analyses were performed using GraphPad Prism 9 software (GraphPad Software Inc., Boston, MA, USA). The level of significance was indicated by ns (not significant), $p>0.05$, $^{*}P<0.05$, $^{**}P<0.01$, $^{***}P<0.001$, and $^{****}P<0.0001$.

Results

TER inhibits cell viability and induces apoptosis in melanoma cells

To detect the viability of cells after TER treatment, UmUc-3 (Bladder Cancer cells), QBC939 (Cholangiocarcinoma cells), Hela (Breast Cancer cells), HepG2 (Hepatocellular carcinoma cells), A375 (melanoma cells) and Hacat (Immortalized skin keratinocytes) were treated with different doses of TER, and tested by MTT assay. Among the six types of human tumor cells and immortalized cells, TER demonstrated the most pronounced inhibitory impact on cell viability in A375 cells (Figure S1A). A comparable phenomenon was observed in another melanoma cell line, M14. Following a 48-hour treatment with 2.0 μg/ml TER, the viability of A375 and M14 cells was reduced to nearly 50%, while HepG2 cells exhibited an inhibition of approximately 25% (Fig. 1A). Crystalline violet staining also visualized the reduced viability of A375 cells (Fig. 1B). Furthermore, the impact of TER on A375 cell invasion was investigated. Transwell experiments demonstrated that the invasive capacity of A375 cells was diminished with the elevation of TER concentration (Figure S1B). Additionally, the expressions of proteins β-catenin, MMP2, and VCAM1, which are associated with cell migration and invasion, also decreased with increasing TER concentration (Figure S1C).

To elucidate the mechanism underlying the potent inhibitory effect of TER on A375 cells and the discrepancies in its action across diverse tumor cell lines, we employed HepG2 as a control. Morphological observations revealed a notable reduction in the viability of A375 cells following TER treatment, accompanied by the formation of small vesicles around the cells. However, this phenomenon was not observed in HepG2 cells (Fig. 1C). In a series of seven distinct cell death inhibitor treatments, it was observed that the combination of BHA (antioxidant) and z-VAD-fmk (pan-caspase inhibitor) pretreatment with subsequent co-culture with TER resulted in a significant increase in the survival of A375 cells (Figure S1D). These observations suggest that apoptosis may have occurred in A375 cells treated with TER [23]. Subsequently, TER-treated A375 and HepG2 cells were double-stained with Annexin V/PI and analyzed by flow cytometry, which is regarded as an effective method for detecting apoptosis [24, 25]. The findings revealed that TER treatment resulted in phosphatidylserine ectopia in a considerable number of A375 cells, a phenomenon that was not observed in HepG2 cells (Fig. 1D and E). These findings indicate that apoptosis is occurring in A375 cells.

Moreover, in comparison to cisplatin, an alternative chemotherapeutic agent that induces apoptosis in cells, TER-treated A375 cells exhibited a reduction in LDH release and no dose-dependent effect (Fig. 1F and G). The discrepancy in LDH release from A375 cells between the two drugs indicates that they may exert inhibitory effects on A375 cell viability through disparate mechanisms.

p53 plays an important role in TER-induced apoptosis

The aforementioned experiments demonstrated that substantial apoptosis was observed in TER-treated A375 cells. To elucidate the mechanism by which TER induces apoptosis in A375 cells, we conducted transcriptome sequencing on TER-treated A375 cells and subsequently analyzed the alterations in the gene expression profiles of the A375 cells. The results demonstrated that the p53 signaling pathway was markedly upregulated in TER-treated A375 cells (Fig. 2A and B). In addition to alterations in gene expression profiles and an increase in p53 protein levels, we also observed the cleavage of key proteins involved in the apoptotic pathway (PARP1, CASP7, CASP3, and GSDME) following TER treatment (Fig. 2C).

To gain further insight into the function of p53 in TER-induced apoptosis, we conducted a gene knockout experiment in A375 cells. The results demonstrated that the tolerance of A375 cells to TER was markedly enhanced following p53 knockout (Fig. 2D). The cleavage of PARP1, CASP7, CASP3, and GSDME induced by TER was significantly reduced in p53 knockout cells (Fig. 2E), and apoptosis was also diminished (Fig. 2F and G). These findings indicate that p53 is a critical mediator of TER-induced apoptosis.

TER induces BAX/FAS overexpression and CASP3 activation through p53 upregulation

As illustrated in Fig. 3A and B, treatment with TER resulted in an elevation in the expression of the apoptosis-related genes BAX and FAS at both the RNA and protein levels in A375 cells. These genes represent downstream targets of the p53 signaling pathway. Following p53 knockout, the alterations in BAX and FAS expression resulting from TER treatment were no longer evident, indicating that p53 is a prerequisite for the observed upregulation of these genes (Fig. 3B). To ascertain the functional consequences of increased BAX and

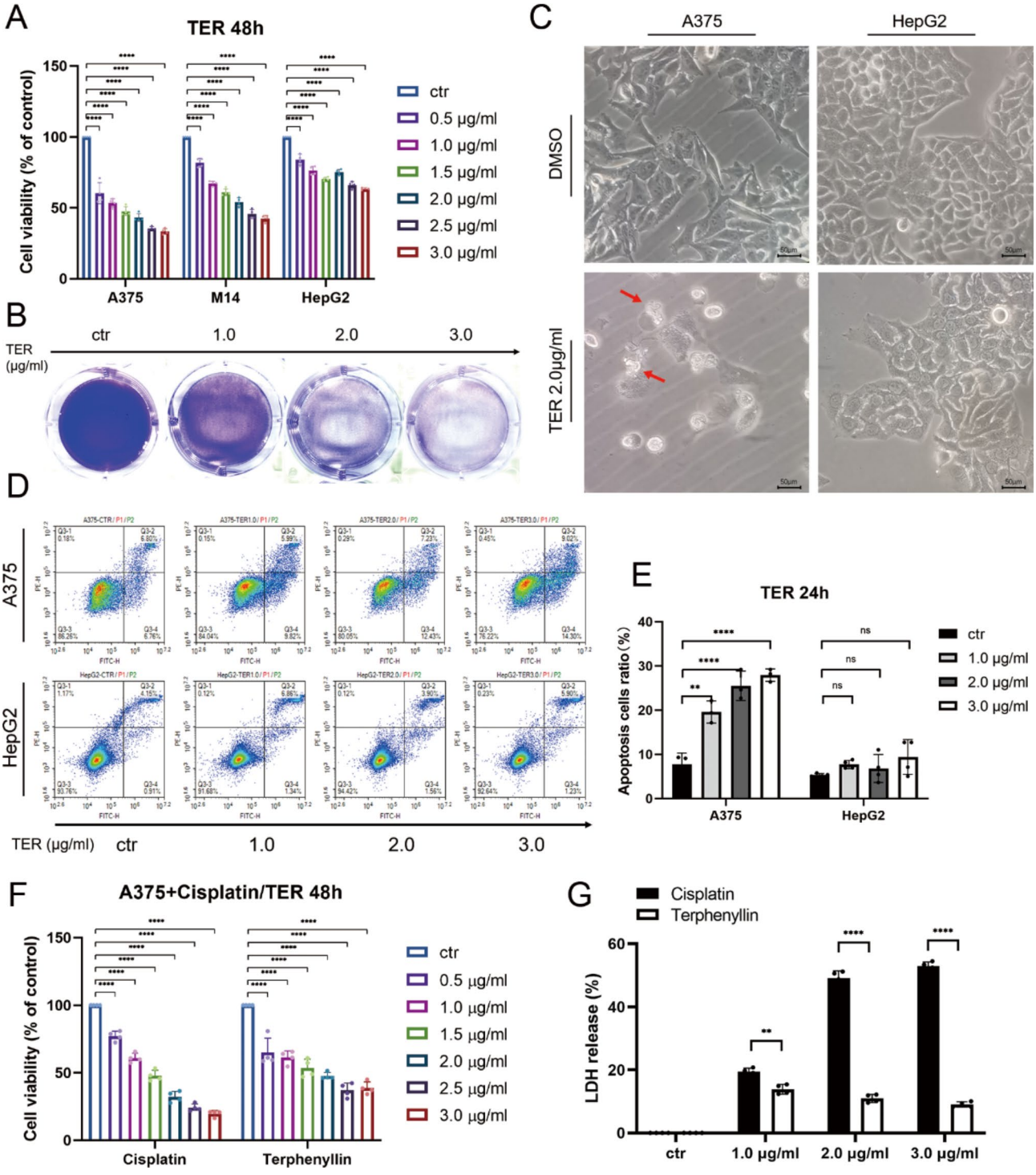

Fig. 1 TER inhibits cell viability and induces apoptosis in melanoma cells. (A) A375, M14, and HepG2 were treated with different doses (0.5, 1.0, 1.5, 2.0, 2.5 and 3.0 μg/ml) of TER for 48 h, after which cell viability was determined via the MTT assay ($n = 4$). (B) Detection of A375 cell survival by crystal violet staining after 48 h of treatment with different doses of TER. (C) Representative bright field microscopy images of A375 and HepG2 cells treated with 2 μg/ml TER for 48 h. (D, E) A375 and HepG2 cells were exposed to different doses of TER (0, 1.0, 2.0 and 3.0 μg/ml) for 24 h, followed by Annexin V-FITC/PI staining and flow cytometry analysis ($n = 4$). A representative density plot of Annexin V-FITC/PI staining is shown in Fig. 1D. (F, G) A375 cells were treated with different doses of cisplatin and TER for 48 h, after which LDH release and cell viability were determined ($n = 4$). Data in A, E, F and G are shown as mean + SEM. Ns: not significant, $p > 0.05$, *$p < 0.05$, **$p < 0.01$, ***$p < 0.001$, ****$p < 0.0001$

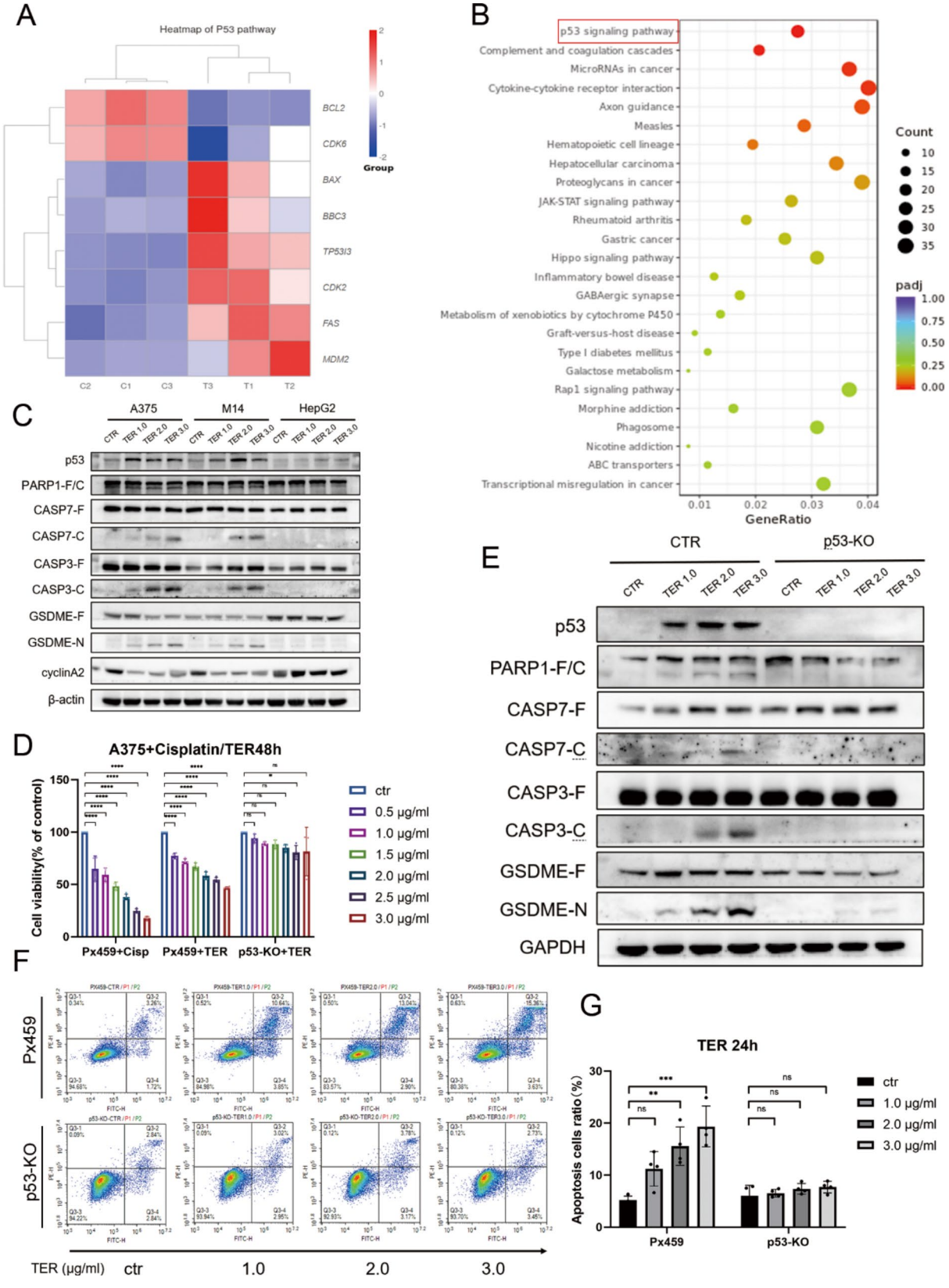

Fig. 2 (See legend on next page.)

(See figure on previous page.)

Fig. 2 p53 plays an important role in TER-induced apoptosis. (A, B) Heatmap showing the differential gene expression activated by p53 in control and TER-treated A375 cells. Bubble plots showing pathways associated with genes differentially expressed between control and TER-treated A375 cells, identified by KEGG pathway analysis of RNA-seq data ($n=3$). (C) Cells were exposed to different doses of TER (1.0, 2.0 and 3.0 μg/ml), and SDS–PAGE and protein blotting were performed to detect the protein expression of p53 and CyclinA2 as well as the cleavage of PARP1, CASP3, CASP7 and GSDME ($n=3$). (D) Cells were treated with different doses (0.5, 1.0, 1.5, 2.0, 2.5 and 3.0 μg/ml) of cisplatin or TER, and then assessed by MTT assay ($n=4$). (E) A375 control and p53-KO cell lines were treated with different doses (0, 1.0, 2.0 and 3.0 μg/ml) of TER, and the cleavage of the PARP1, GSDME and CASP3/7 was detected via SDS–PAGE and protein blotting ($n=3$). (F, G) A375 and P53-KO cells were treated with different doses (0, 1.0, 2.0 and 3.0 μg/ml) of TER for 24 h, followed by Annexin V-FITC/PI staining and flow cytometry analysis ($n=4$). A representative density plot of Annexin V-FITC/PI staining is shown in Fig. 2G. Data in D and G are shown as mean + SEM. Ns: not significant, $p>0.05$, *$p<0.05$, **$p<0.01$, ***$p<0.001$, ****$p<0.0001$

FAS expression, we proceeded to overexpress these proteins individually in A375 cells. As illustrated in Fig. 3C and S2A, cleavage of PARP1, CASP3, and GSDME was evident in both BAX- and FAS-overexpressing cells. However, overexpression of other upregulated genes identified in the RNA-seq results did not elicit this phenomenon. These findings suggest that the upregulation of both BAX and FAS can contribute to the activation of apoptotic pathways.

Moreover, the subcellular localization of cytochrome c, a pivotal factor in apoptosis, was investigated. The results demonstrated that cytochrome c was released from the mitochondria into the cytoplasm and partially into the nucleus in TER-treated A375 cells (Fig. 3D and E), a finding that was further corroborated by the transcriptome data (Fig. 3F). Other proteins linked to mitochondrial membrane permeabilization (MMP), including End G and AIF, were also observed to be released from mitochondria (Fig. 3D). Additionally, gene set enrichment analysis (GSEA) revealed an enrichment of genes associated with mitotic DNA integrity checkpoints, indicating that TER treatment may influence the efficiency of DNA replication in A375 cells (Fig. 3G).

TER induces A375 cell cycle arrest in G2 and S phases

Following the enrichment of gene expression data associated with DNA replication checkpoints, an investigation was conducted into the specific mechanism underlying the inhibition of proliferation in TER-treated A375 cells. As illustrated in Fig. 4A, the cell colony formation assay demonstrated a decline in cell proliferative capacity with elevated TER concentrations. The distribution of Ki67, a protein that plays a role in preventing chromosome collapse during mitosis [26, 27], was also examined. In contrast to the control group, in which Ki67 was observed to aggregate around chromosomes, Ki67 was found to be evenly distributed throughout the nucleus in TER-treated A375 cells, and cell division was no longer evident within the field of view (Fig. 4C). This result indicated that the DNA replication process is indeed altered in TER-treated A375 cells.

To investigate the molecular mechanism underlying this process, we examined the expression of cell cycle-related proteins. The results showed that the inhibitory effect of TER on Cyclin A2 expression increased with the increase of TER concentration and was alleviated after p53 knockout (Fig. 4D). Cyclin A2 can activate CDK2 and facilitate the transition between the G1/S and G2/M phases of the cell cycle (Fig. 4B). The inhibition of Cyclin A2 expression may lead to blockage of the G2/M phase and an increase in the number of tetraploid cells (in G2 and S phase) [28–30]. This phenomenon was corroborated by flow cytometry analysis of A375 cells that treated with a low dose of TER (Fig. 4E and F). The results demonstrate that TER can block the cell cycle of A375 cells in G2 and S phases, which may be related to the decreased expression of Cyclin A2 induced by p53.

Knockout of CASP3 converts TER-induced apoptosis into cell necrosis

Although we observed cleavage of CASP3, a key protein involved in apoptosis, following TER treatment, it is important to note that knockout of CASP3 did not alleviate the TER-induced reduction in A375 cell viability (Fig. 5A). Interestingly, this reduction in cell number is not due to apoptosis but to necrosis. This was evidenced by the migration of the cell population toward the PI-positive and Annexin V-negative group after TER treatment in the CASP3-KO cell line. Moreover, the percentage of apoptotic cells (Annexin V-positive) was reduced after CASP3 knockout (Fig. 5B and C). In situ Annexin V-FITC/PI staining also showed that TER could directly lead to necrosis in CASP3-KO cells, because the cell membrane of TER-treated CASP3-KO cells did not undergo phosphatidylserine ectopia (Fig. 5D). Moreover, knockout of CASP3 significantly promoted TER-induced LDH release from A375 cells in a dose-dependent manner, providing further evidence for the occurrence of necrosis (Fig. 5E).

TER induces GSDME-dependent cell pyroptosis via activated CASP3 in A375 cells

As illustrated in Fig. 6A, the TER-induced cleavage band corresponding to GSDME was entirely absent in the CASP3 knockout cell line, whereas the cleavage band of PARP1 remained. This indicates that PARP1 is not cleaved by CASP3, but rather by other downstream proteins induced by p53 in A375 cells. The role of GSDME in TER-induced apoptosis was subsequently investigated. The results demonstrated that the knockout of GSDME

resulted in a notable elevation in apoptosis (Fig. 6B and C) and a reduction in TER-induced LDH release (Fig. 6D), which exhibited a mechanism of death induction comparable to that observed in colon cancer cells treated with lobaplatin [31].

Prior research has indicated that CASP3 facilitates the cleavage of GSDME, thereby enabling the progression of drug-induced apoptosis to secondary necrosis or pyroptotic cell death [32]. Chemotherapeutic agents can induce cellular pyroptosis via the BAK/BAX-caspase-3-GSDME pathway [32, 33]. To ascertain whether this pathway is implicated in TER-induced apoptosis, two sets of co-expression experiments were conducted in A375 cells, BAX/GSDME group and FAS/GSDME group. The results showed that both co-expression groups resulted in increased LDH release from A375 cells and the release of LDH in both groups was effectively alleviated by the caspase inhibitor Z-VAD-fmk (Fig. 6E). Besides, it was difficult to observe intact co-expressed cells in the BAX/GSDME group (Fig. 6F). The above results suggest that the cellular pyroptosis mediated by the BAX-CASP3-GSDME pathway is also present in TER-induced A375 cells.

Enzymes with upregulated expression in the amino and nucleotide sugar metabolism pathways are not directly involved in TER-induced cell death

Previous studies have shown that TER has significant α-glucosidase inhibitory activity [19]. To ascertain whether alterations in metabolic pathways are implicated in TER-induced cell death, an examination of the metabolome of A375 cells following TER treatment was conducted. It was observed that the metabolic pathways of amino sugars and nucleotides were significantly upregulated following TER treatment (Fig. 7A and B). To gain further insight into the molecular mechanisms underlying these metabolic alterations, we examined the expression of pivotal enzymes involved in the pathway. Our findings revealed a significant upregulation in the expression of *GALK1*, *GALE*, and *GALT* (Fig. 7C), which aligns with the results of transcriptome sequencing (Fig. 7D). To ascertain the function of these enzymes in TER-induced cell viability and apoptosis, we proceeded to overexpress them in A375 cells. However, no changes were observed in the cleavage of apoptosis-related downstream proteins upon overexpression of *GALK1*, *GALE*, or *GALT* (Figs. 3D and 7F, and S2B). Furthermore, no differences were observed in the distribution of KI67 following overexpression (Fig. 7E).

Discussion

The findings of our study indicate that TER exerted a significant inhibitory effect on cell viability in A375 cells. This was achieved through a dual mechanism involving promotion of cell death and inhibition of cell proliferation. TER promoted an increase in the expression of p53 protein in A375 cells, which in turn activated BAX. The activation of BAX resulted in the release of cytochrome C from mitochondria, which in turn triggered the activation of caspase-3 through the intrinsic apoptotic pathway, thereby significantly contributing to the development of apoptosis in A375 cells. On the other hand, up-regulated p53 inhibits the expression of Cyclin A2, a protein that is important for the G1/S and G2/M phases transition during the cell cycle [28–30]. Similar blockage of the cell cycle in G2 and S phases was observed in TER-treated A375 cells (Fig. 8).

It has been reported that certain chemotherapeutic agents can induce cellular pyroptosis through the activation of the CASP3-GSDME pathway [31, 34, 35]. GSDME is cleaved by caspase-3 specifically in its linker, generating a GSDME-N fragment that perforates membranes and thereby induces pyroptosis [34]. Under sterile conditions, bile acids can also trigger CASP3-GSDME induced pyroptosis by promoting mitochondrial permeability transition (MPT) [36]. In this study, we observed that the overexpression of BAX and GSDME markedly enhanced LDH release in A375 cells, which was effectively attenuated by the introduction of a pan-caspase inhibitor. This suggests that TER-induced cell death is not attributable to a single mode of cell death, and that apoptosis and pyroptosis coexist in TER-induced A375 cells.

It has long been assumed that cell death pathways function in parallel. However, a growing body of evidence suggests that apoptosis, necrotic apoptosis, and pyroptosis are closely linked [37, 38]. Even in the same cell, these three pathways can be cross-regulated with each other by a multi-protein complex called the PANoptosome [39, 40]. In mice, elimination of MLKL to prevent lethal necrotic apoptosis is followed by ASC and caspase-1 signalling that contribute to lethality [41]. Ileitis in mice with FADD-deficient intestinal epithelial cells can be driven by necroptosis or GSDMD-dependent pyroptosis [42]. This cross-regulation was also found in our study. Knockout of GSDME promoted TER-induced apoptosis, while knockout of CASP3 converted TER-induced apoptosis into cell necrosis.

Ki67 is one of the most widely used proliferation markers in oncology [43]. It is function as a component of the mitotic chromosome periphery that prevents chromosomes from collapsing into individual chromatin clusters after nuclear membrane disassembly [26]. During interphase Ki67 binds primarily to the densely packed chromatin fraction at the periphery of the nucleolus, while during mitosis it is localized around the chromosomes [44]. Interestingly, in TER-treated A375 cells, although we observed a significant inhibition of cell proliferation, no reduction in Ki67 expression occurred. We speculate

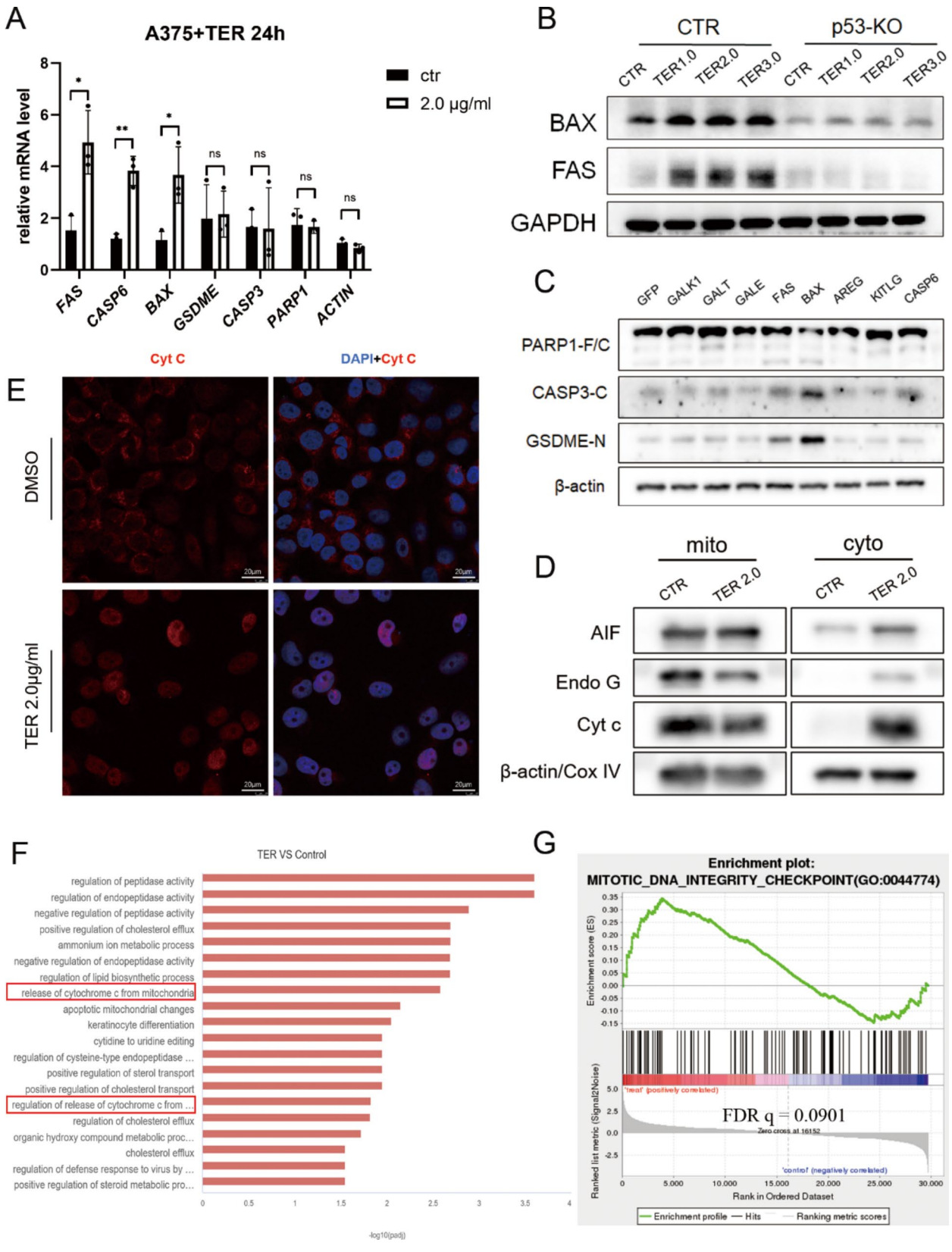

Fig. 3 (See legend on next page.)

(See figure on previous page.)

Fig. 3 TER induces BAX/FAS overexpression and CASP3 activation through p53 upregulation. (A) Relative expression levels of the *FAS*, *BAX*, *CASP6*, *CASP3*, *GSDME* and *PARP1* mRNAs in A375 cells after treatment with TER (2 μg/ml) for 24 h. Gene expression was assessed via qPCR. The error bars represent the means ± SDs ($n = 3$). (B) Cells were treated with different doses (0, 1.0, 2.0 and 3.0 μg/ml) of TER, and the expression of apoptosis-related proteins (FAS and BAX) was detected via SDS–PAGE and protein blotting ($n = 3$). (C) Overexpression of signaling pathway-related genes (*FAS*, *BAX*, *CASP6* and *ARGE*) and metabolism-related genes (*GALK1*, *GALT*, *GALE* and *KITLG*) in A375 cells, and cleavage of PARP1, CASP3 and GSDME proteins was detected by SDS–PAGE and protein blotting ($n = 3$). (D) A375 cells were treated with TER (2.0 μg/ml) to detect differences in the distribution of mitochondrial and intracytoplasmic proteins between the experimental and control groups ($n = 3$). (E) A375 cells were treated with TER (2.0 μg/ml) for 24 h to determine the distribution of cytochrome C (red) in the experimental and control groups. (F) GO enrichment analysis ($n = 3$) of the upregulated mRNA DEGs in biological processes (BPs). (G) Differentially expressed genes (TER2.0 μg/ml vs. control, $n = 3$) were enriched for "Mitotic DNA integrity Checkpoint" as established by GESA. Data in A is shown as mean + SEM. Ns: not significant, $p > 0.05$, *$p < 0.05$, **$p < 0.01$, ***$p < 0.001$, ****$p < 0.0001$

that this is related to the period of Ki67 expression. Iain Miller et al. tracked Ki67 levels under endogenous control in single cells over time and found that Ki67 accumulation occurs only during S, G2, and M phases and continued to be degraded upon entry into the G1 and G0 phases [45]. Given that TER inhibited A375 cells primarily during the G2 and S phases, when the cells had already completed Ki67 accumulation, the expression of Ki67 detected under immunofluorescence was not affected and even exhibited a tendency to increase. Nevertheless, additional research is required to ascertain the function of Ki67 during this phase.

E-type cell cycle proteins, collectively known as cell cycle protein E, represent key components of the core cell cycle machinery [46]. In mammalian cells, two E-type cell cycle proteins, E1 and E2, activate cyclin-dependent kinase 2 (CDK2) and drive cell cycle progression by phosphorylating several cellular proteins [47, 48]. Overexpression of E1 results in replication stress, mitotic abnormalities, and increased sensitivity to replication checkpoint inhibitors [49]. In this study, we also found a slight upregulation of cyclin E1 after TER treatment, which was more significant after p53 knockout. Notably, although TER affected the expression of cyclin E1 to some extent, p53 knockout did not eliminate or reverse the expression trend of cyclin E1. It indicates that the expression trend change of cyclin E1 may not be directly regulated by p53, which is also consistent with the study of Zeng et al. Previously, they found similar levels of cyclin E1 expression in p53-positive and p53-knockout RPE1 cells induced by doxycycline [50].

PARP1 is a protein that plays multiple roles in the cell, including by modifying nuclear proteins, repairing DNA damage, and promoting apoptosis [51, 52]. It has been shown that a truncated form of PARP1 can activate RNA Pol III and induce IFN-β production and apoptosis [53], in which truncated 89 KB PARP1 can act as a cytoplasmic PAR carrier and induce AIF release from mitochondria [54]. It was previously reported that PARP1 is one of the downstream substrates for CASP3 activation [55, 56]. However, in our study, we found that knockout of CASP3 did not prevent TER-induced cleavage of PARP1, implying that another mode of PARP1 cleavage exists in TER-treated A375 cells.

In summary, TER not only inhibited A375 cell proliferation, but also induced programmed cell death (PCD) through the P53-BAX-CASP3 pathway. Activated CASP3 in this pathway promotes apoptosis on the one hand, and on the other hand, it continues to cleave GSDME to trigger pyroptosis, and ultimately stimulates A375 cell death in the form of apoptosis and pyroptosis coexistence. It is interesting to note that neither CASP3 knockout nor GSDME knockout could rescue TER-induced cell death, and TER-induced cell death could be significantly alleviated only when the upstream protein of this pathway, p53, was knocked out. This suggests that CASP3 and GSDME in this pathway regulate the manner of cell death, rather than determining whether cell death occurs. This process can be likened to the flow of water in a river. Once the main valve is opened, the valve situated further downstream will determine the direction of the river's flow, but will not affect the river's overall tendency to flow downstream.

Conclusions

To investigate the mechanism by which TER inhibits melanoma cell viability, we sequenced the transcriptome of TER-treated A375 cells and found a significant upregulation of the p53 signaling pathway. We demonstrated p53-BAX/FAS-CASP3-GSDME as the main mechanism of TER-induced A375 cell death. Compared with the broad-spectrum chemotherapeutic agent-cisplatin, TER induced A375 cell death in a milder manner and showed some cell specificity. This lays the foundation for TER as a potential anti-melanoma drug in the future. In addition, we found that the knockout of CASP3 and GSDME of the pathway did not prevent TER-induced cell death, but rather shifted the cell death to another mode, which also provides valuable information for the apoptosis and pyroptosis studies.

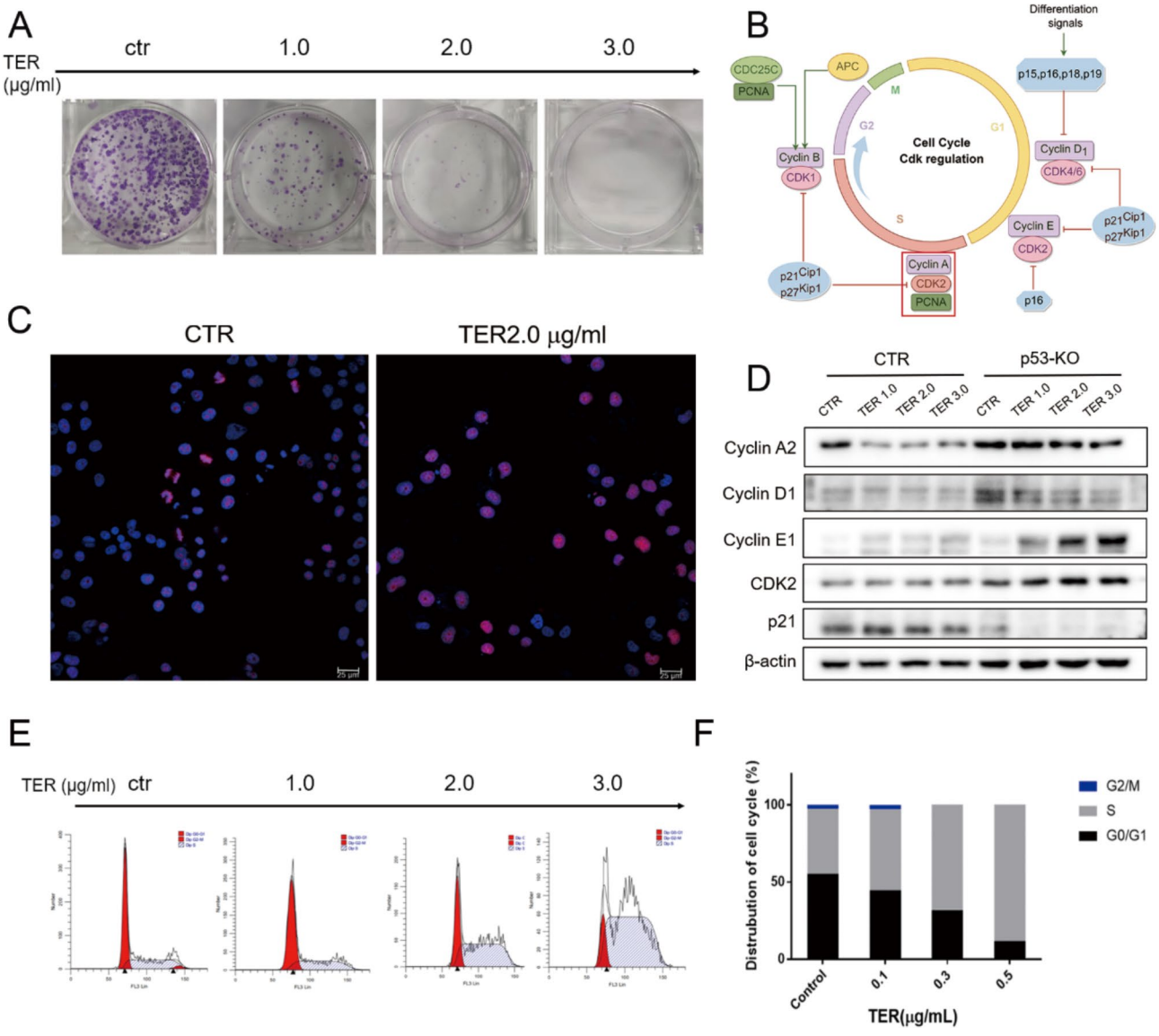

Fig. 4 Inhibition of cell proliferation by TER is associated with a decrease in CyclinA2. (A) A plate colony formation assay was used to detect cell colony formation ability, and the images show the results of Giemsa staining. (B) Cell cycle CDK regulation pattern map. Drawing by Figdraw. (C) A375 cells were treated with TER (2 μg/ml) for 24 h, and the images show the distribution of Ki67 (red) protein. (D) A375 control and p53-KO cell lines were treated with different doses (0, 1.0, 2.0 and 3.0 μg/ml) of TER, and the image shows the expression of cell cycle-related proteins (Cyclin A2, Cyclin D1, Cyclin E1, CDK2, and p21). ($n=3$) (E, F) A375 cells were exposed to lower doses of TER (0.1, 0.3 and 0.5 μg/ml) for 48 h. The cells were labeled with PI and detected by flow cytometry

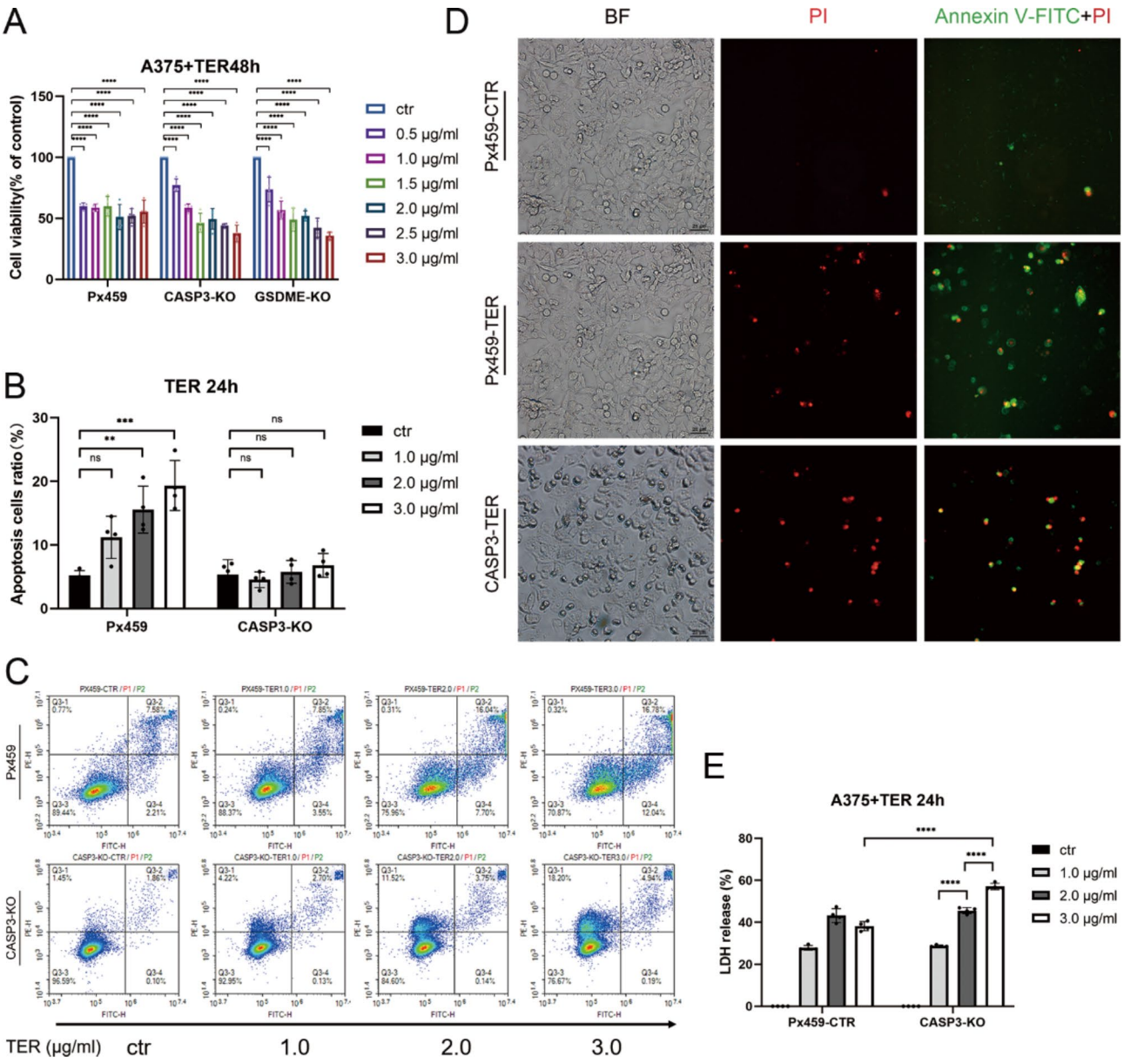

Fig. 5 Knockout of CASP3 converts TER-induced apoptosis into cell necrosis. (A) A375, CASP3-KO and GSDME-KO cell lines were treated with different doses of TER (0.5, 1.0, 1.5, 2.0, 2.5 and 3.0 μg/ml) for 48 h, and then cell viability was determined via MTT assay ($n=4$). (B, C) A375 and CASP3-KO cells were treated with different doses (0, 1.0, 2.0 and 3.0 μg/ml) of TER for 24 h, followed by Annexin V-FITC/PI staining and flow cytometry analysis ($n=4$). A representative density plot of Annexin V-FITC/PI staining is shown in Fig. 5E. (D) A375 and CASP3-KO cells were treated with TER (2.0 μg/ml) or DMSO for 24 h, and then labeled with Annexin V-FITC/PI for observation under a fluorescence microscope. (E) A375-Control/CASP3-KO cells were treated with different doses of TER (0, 1.0, 2.0, and 3.0 μg/ml) for 24 h, after which LDH release was determined ($n=4$). Data in A, B and E are shown as mean + SEM. Ns: not significant, $p>0.05$, *$p<0.05$, **$p<0.01$, ***$p<0.001$, ****$p<0.0001$

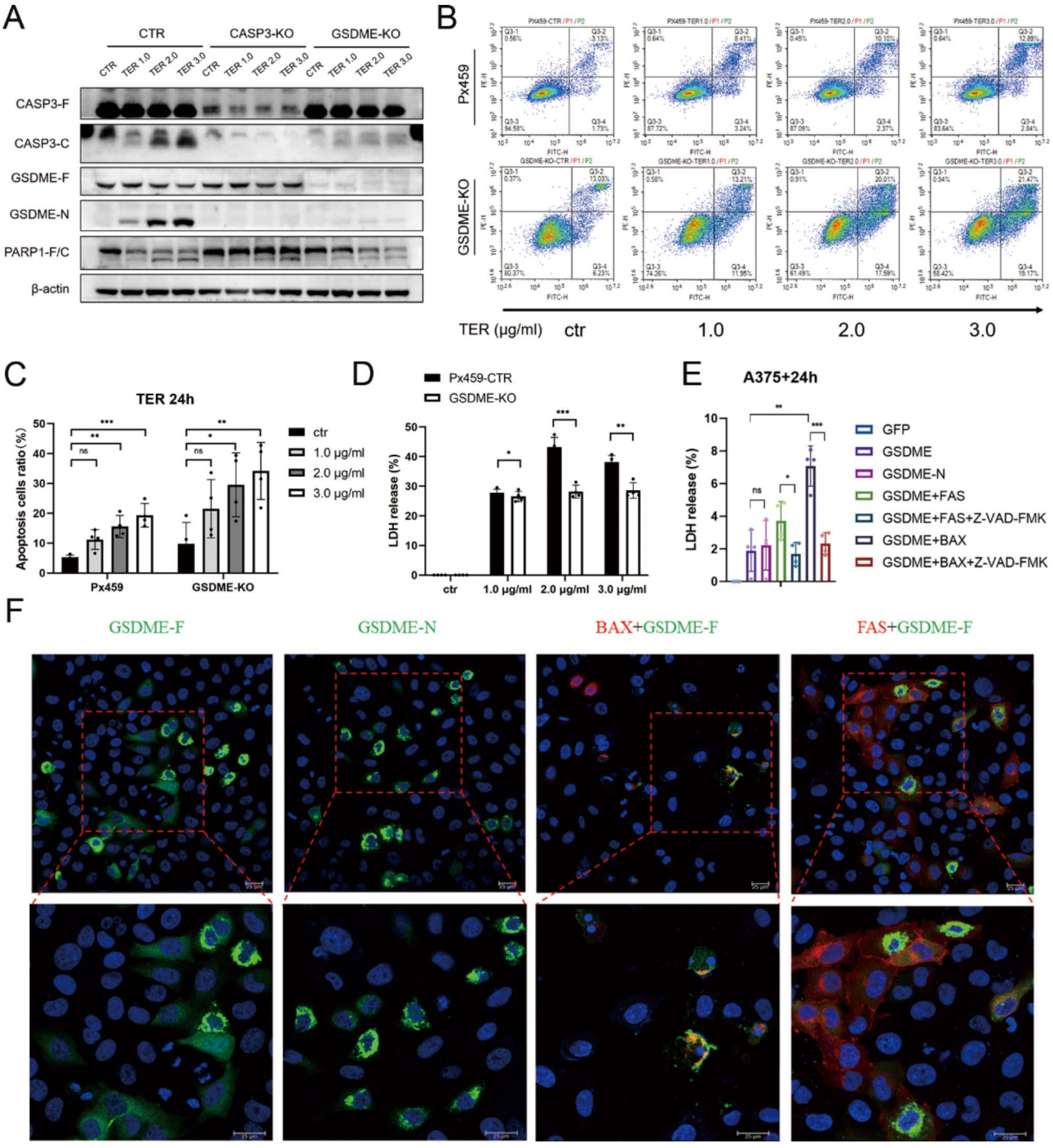

Fig. 6 TER induces GSDME-dependent cell pyroptosis via activated CASP3 in A375 cells. (A) A375 control, CASP3-KO and GSDME-KO cell lines were treated with different doses of TER (0, 1.0, 2.0 and 3.0 μg/ml), and cleavage of PARP1, CASP3 and GSDME was detected by SDS–PAGE and protein blotting ($n=3$). (B, C) A375 and GSDME-KO cells were treated with different doses (0, 1.0, 2.0 and 3.0 μg/ml) of TER for 24 h, followed by Annexin V-FITC/PI staining and flow cytometry analysis ($n=4$). A representative density plot of Annexin V-FITC/PI staining is shown in Fig. 6B. (D) A375-Control/GSDME-KO cells were treated with different doses of TER (0, 1.0, 2.0, and 3.0 μg/ml) for 24 h, after which LDH release was determined ($n=4$). (E) FAS or BAX was co-expressed with GSDME, the cells were treated with a caspase inhibitor (Z-VAD-FMK), and LDH release was determined ($n=4$). (F) FAS-HA or BAX-HA (red) was co-expressed with GSDME-GFP (green), and cell morphology and protein localization were detected by immunofluorescence. Data in C, D and E are shown as mean + SEM. Ns: not significant, $p>0.05$, *$p<0.05$, **$p<0.01$, ***$p<0.001$, ****$p<0.0001$

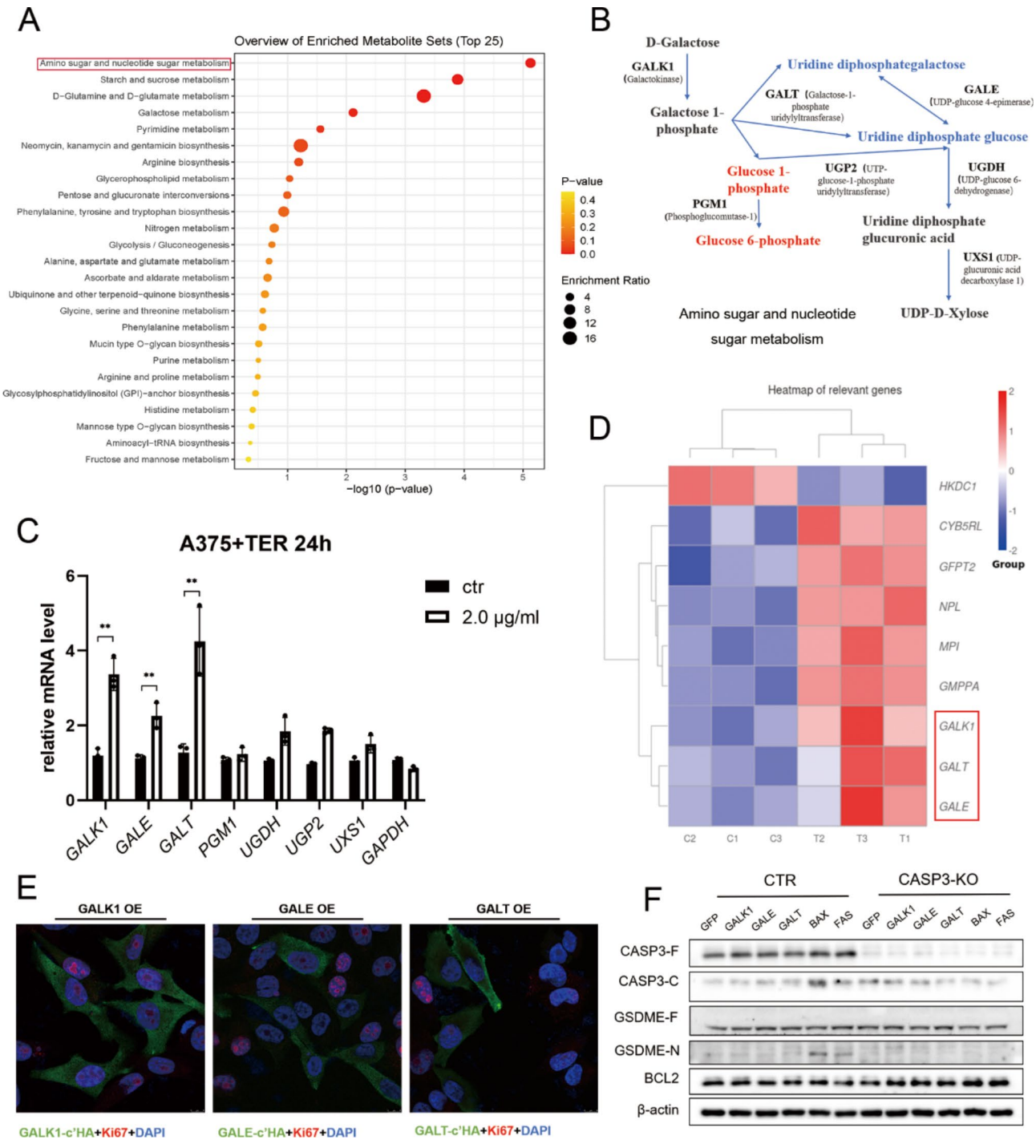

Fig. 7 Enzymes with upregulated expression in the amino and nucleotide sugar metabolism pathways are not directly involved in TER-induced cell death. (A) Metabolic pathway enrichment analysis of upregulated metabolites in A375 cells after 24 h of TER treatment ($n=3$). (B) Schematic representation of amino sugar and nucleotide sugar metabolism in cells. Red: upregulated metabolites; Blue: downregulated metabolites. (C) A375 cells were treated with TER (2 μg/ml) for 24 h, after which mRNA levels of key enzymes involved in intracellular amino sugar and nucleotide sugar metabolism were detected via RT–qPCR ($n=3$). (D) TER treatment of A375 cells for 24 h, identified by KEGG (gene set enrichment analysis) typical pathway analysis of RNA-seq data. Heatmap showing the differences in the expression of key enzymes involved in amino sugar and nucleotide sugar metabolism in control and TER-treated A375 cells. (E) Overexpression of GALK1/GALE/GALT in A375 cells and detection of KI67 expression. Green: overexpressed genes; Red: KI67; Blue: DAPI. (F) Overexpression of GALK1/GALE/GALT/BAX/FAS proteins in A375 and CASP3-KO cells, and cleavage of CASP3 and GSDME proteins was detected by SDS–PAGE and protein blotting. Data in C is shown as mean + SEM. Ns: not significant, $p > 0.05$, *$p < 0.05$, **$p < 0.01$, ***$p < 0.001$, ****$p < 0.0001$

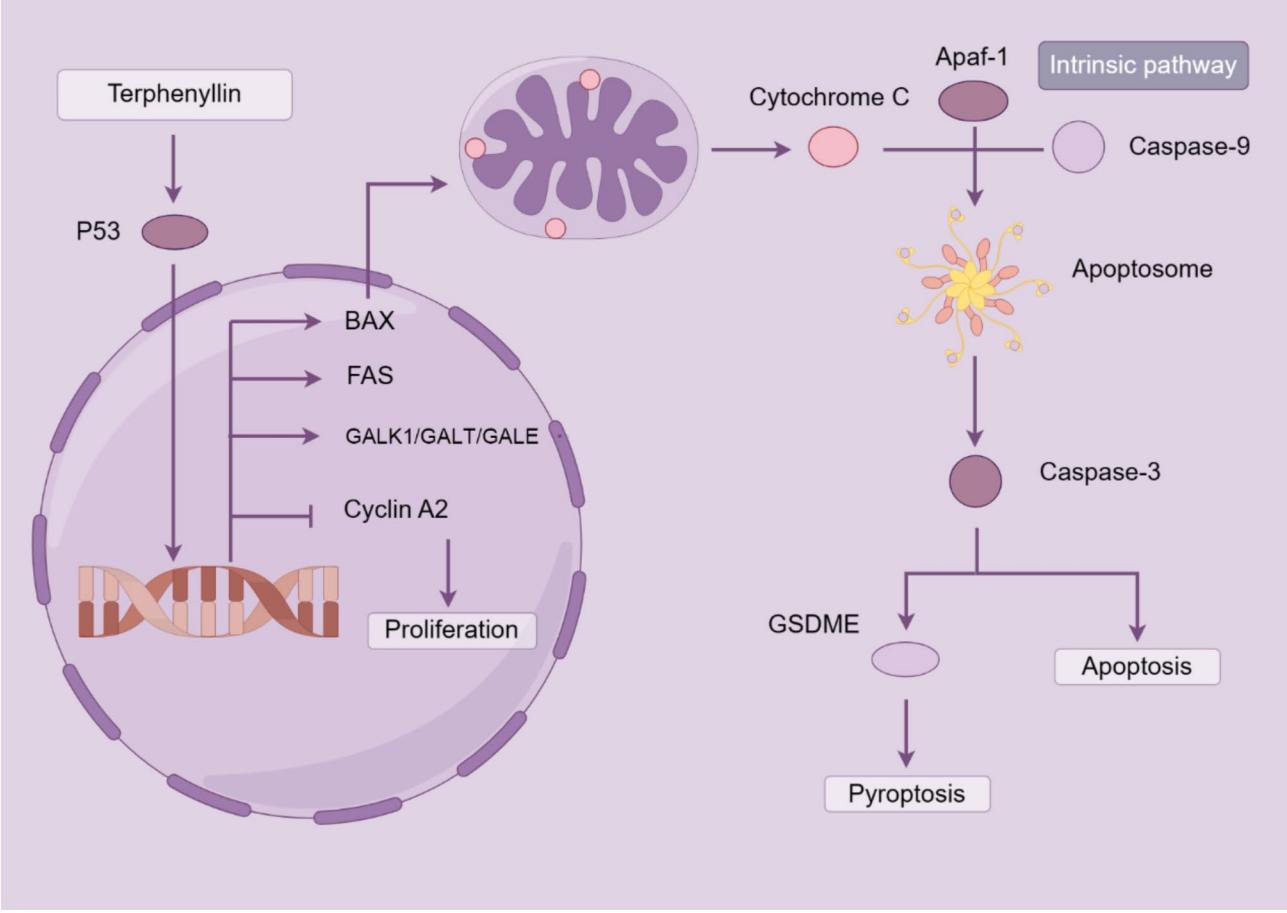

Fig. 8 Summary of the mechanisms by which TER inhibits cell viability in A375 cells

Abbreviations

TER	Terphenyllin
PARP1	Poly (ADP-ribose) polymerase 1
CASP7	Caspase 7
CASP3	Caspase 3
GSDME	Gasdermin E (DFNA5)
p53	Tumor protein p53
p21	Cyclin dependent kinase inhibitor 1 A
BCL2	BCL2 apoptosis regulator
FAS	Fas cell surface death receptor
BAX	BCL2 associated X
CCNA2	Cyclin A2
CCND1	Cyclin D1
AIF	Apoptosis inducing factor mitochondria associated 1
Endo G	Endonuclease G
Cyt C	Cytochrome c
Cox	IV Cytochrome c oxidase subunit 4
Ki67	Proliferation marker protein Ki-67
BRAF	B-Raf proto-oncogene, serine/threonine kinase

Supplementary Information

The online version contains supplementary material available at https://doi.org/10.1186/s12964-024-01784-7.

Supplementary Material 1

Supplementary Material 2

Supplementary Material 3

Supplementary Material 4

Supplementary Material 5

Acknowledgements
Not applicable.

Author contributions
Wei Wu: Investigation, Designed and performed experiments, analyzed data, Writing-original draft & editing. Mengyuan Wu, Ting Dai: Investigation, performed experiments, analyzed data. Lina Ke, Yan Shi: Writing-review & editing, Supervision. Jin Hu: Funding acquisition, Writing - review & editing. Qin Wang: Conceptualization, Funding acquisition, Writing - review & editing, Supervision. All authors reviewed and approved the final manuscript.

Funding
This study was supported by the Technology Innovation Center for Exploitation of Marine Biological Resources, MNR (TICMBR202404), the Natural Science Foundation of Xiamen, China (3502Z202373014), the National Natural Science Foundation of China (31870780 and 82371419), and the Xiamen Southern Oceanographic Center (16PFW008SF15 and 21CZP002HJ05).

Data availability
The datasets generated and analyzed during the current study are available in the NCBI SRA database. under Bioproject # PRJNA1075735, Biosamples SAMN39918152-SAMN39918157.

Declarations

Ethics approval and consent to participate
Not applicable.

Consent for publication
Not applicable.

Competing interests
The authors declare no competing interests.

Received: 4 July 2024 / Accepted: 9 August 2024
Published online: 21 August 2024

References

1. Shain AH, Bastian BC. From melanocytes to melanomas. Nat Rev Cancer. 2016;16:345–58. https://doi.org/10.1038/nrc.2016.37.
2. Saginala K, Barsouk A, Aluru JS, Rawla P, Barsouk A. Epidemiology of Melanoma. Med Sci (Basel). 2021;9:63. https://doi.org/10.3390/medsci9040063.
3. Schadendorf D, van Akkooi ACJ, Berking C, Griewank KG, Gutzmer R, Hauschild A, et al. Melanoma Lancet. 2018;392:971–84. https://doi.org/10.1016/S0140-6736(18)31559-9.
4. Narayanan DL, Saladi RN, Fox JL. Ultraviolet radiation and skin cancer. Int J Dermatol. 2010;49:978–86. https://doi.org/10.1111/j.1365-4632.2010.04474.x.
5. Davis LE, Shalin SC, Tackett AJ. Current state of melanoma diagnosis and treatment. Cancer Biol Ther. 2019;20:1366–79. https://doi.org/10.1080/15384047.2019.1640032.
6. Lee C, Collichio F, Ollila D, Moschos S. Historical review of melanoma treatment and outcomes. Clin Dermatol. 2013;31:141–7. https://doi.org/10.1016/j.clindermatol.2012.08.015.
7. Long GV, Swetter SM, Menzies AM, Gershenwald JE, Scolyer RA. Cutaneous melanoma. Lancet. 2023;402:485–502. https://doi.org/10.1016/S0140-6736(23)00821-8.
8. Larkin J, Chiarion-Sileni V, Gonzalez R, Grob JJ, Rutkowski P, Lao CD, et al. Five-year survival with combined Nivolumab and Ipilimumab in Advanced Melanoma. N Engl J Med. 2019;381:1535–46. https://doi.org/10.1056/NEJMoa1910836.
9. Lauss M, Phung B, Borch TH, Harbst K, Kaminska K, Ebbesson A, et al. Molecular patterns of resistance to immune checkpoint blockade in melanoma. Nat Commun. 2024;15:3075. https://doi.org/10.1038/s41467-024-47425-y.
10. Gide TN, Wilmott JS, Scolyer RA, Long GV. Primary and Acquired Resistance to Immune checkpoint inhibitors in metastatic melanoma. Clin Cancer Res. 2018;24:1260–70. https://doi.org/10.1158/1078-0432.CCR-17-2267.
11. Dummer R, Ascierto PA, Gogas HJ, Arance A, Mandala M, Liszkay G, et al. Encorafenib plus Binimetinib versus vemurafenib or encorafenib in patients with BRAF-mutant melanoma (COLUMBUS): a multicentre, open-label, randomised phase 3 trial. Lancet Oncol. 2018;19:603–15. https://doi.org/10.1016/S1470-2045(18)30142-6.
12. Long GV, Hauschild A, Santinami M, Atkinson V, Mandala M, Chiarion-Sileni V, et al. Adjuvant dabrafenib plus Trametinib in Stage III BRAF-Mutated Melanoma. N Engl J Med. 2017;377:1813–23. https://doi.org/10.1056/NEJMoa1708539.
13. Ascierto PA, McArthur GA, Dreno B, Atkinson V, Liszkay G, Di Giacomo AM, et al. Cobimetinib combined with vemurafenib in advanced BRAF(V600)-mutant melanoma (coBRIM): updated efficacy results from a randomised, double-blind, phase 3 trial. Lancet Oncol. 2016;17:1248–60. https://doi.org/10.1016/S1470-2045(16)30122-X.
14. Robert C, Grob JJ, Stroyakovskiy D, Karaszewska B, Hauschild A, Levchenko E, et al. Five-year outcomes with Dabrafenib plus Trametinib in Metastatic Melanoma. N Engl J Med. 2019;381:626–36. https://doi.org/10.1056/NEJMoa1904059.
15. Ascierto PA, Dreno B, Larkin J, Ribas A, Liszkay G, Maio M, et al. 5-Year outcomes with Cobimetinib plus Vemurafenib in BRAFV600 mutation-positive Advanced Melanoma: Extended follow-up of the coBRIM study. Clin Cancer Res. 2021;27:5225–35. https://doi.org/10.1158/1078-0432.CCR-21-0809.
16. Schadendorf D, Dummer R, Flaherty KT, Robert C, Arance A, de Groot JWB, et al. COLUMBUS 7-year update: a randomized, open-label, phase III trial of encorafenib plus binimetinib versus vemurafenib or encorafenib in patients with BRAF V600E/K-mutant melanoma. Eur J Cancer. 2024;204:114073. https://doi.org/10.1016/j.ejca.2024.114073.
17. Bailly C. Anti-inflammatory and anticancer p-terphenyl derivatives from fungi of the genus Thelephora. Bioorg Med Chem. 2022;70:116935. https://doi.org/10.1016/j.bmc.2022.116935.
18. Xu Y, Wang Y, Wu D, He W, Wang L, Zhu W. p-Terphenyls from aspergillus sp. GZWMJZ-055: identification, derivation, antioxidant and alpha-glycosidase inhibitory activities. Front Microbiol. 2021;12:654963. https://doi.org/10.3389/fmicb.2021.654963.
19. Zhang XQ, Mou XF, Mao N, Hao JJ, Liu M, Zheng JY, et al. Design, semisynthesis, α-glucosidase inhibitory, cytotoxic, and antibacterial activities of -terphenyl derivatives. Eur J Med Chem. 2018;146:232–44. https://doi.org/10.1016/j.ejmech.2018.01.057.
20. Yu DH, Qi SM, Guan XQ, Yu WK, Yu XF, Cai MH, et al. Inhibition of STAT3 signaling pathway by Terphenyllin suppresses growth and metastasis of gastric Cancer. Front Pharmacol. 2022;13:870367. https://doi.org/10.3389/fphar.2022.870367.
21. Zhang J, Wang WY, Zhou Y, Yang J, Xu JL, Xu ZY, et al. Terphenyllin suppresses Orthotopic pancreatic tumor growth and prevents metastasis in mice. Front Pharmacol. 2020;11:457. https://doi.org/10.3389/fphar.2020.00457.
22. Sander JD, Joung JK. CRISPR-Cas systems for editing, regulating and targeting genomes. Nat Biotechnol. 2014;32:347–55. https://doi.org/10.1038/nbt.2842.
23. Taylor RC, Cullen SP, Martin SJ. Apoptosis: controlled demolition at the cellular level. Nat Rev Mol Cell Bio. 2008;9:231–41. https://doi.org/10.1038/nrm2312.
24. Vanoers MHJ, Reutelingsperger CPM, Kuyten GAM, Vondemborne AEGK, Koopman G. Annexin-V for Flow Cytometric detection of Phosphatidylserine expression on B-Cells undergoing apoptosis. Blood. 1994;84:A291–291. https://doi.org/.
25. Vermes I, Haanen C, Steffensnakken H, Reutelingsperger C. A novel assay for apoptosis - Flow Cytometric detection of Phosphatidylserine expression on early apoptotic cells using Fluorescein-labeled Annexin-V. J Immunol Methods. 1995;184:39–51. https://doi.org/10.1016/0022-1759(95)00072-I.
26. Cuylen S, Blaukopf C, Politi AZ, Müller-Reichert T, Neumann B, Poser I, et al. Ki-67 acts as a biological surfactant to disperse mitotic chromosomes. Nature. 2016;535:308–12. https://doi.org/10.1038/nature18610.
27. Booth DG, Takagi M, Sanchez-Pulido L, Petfalski E, Vargiu G, Samejima K, et al. Ki-67 is a PP1-interacting protein that organises the mitotic chromosome periphery. Elife. 2014;3:e01641. https://doi.org/10.7554/eLife.01641.
28. Pagano M, Pepperkok R, Verde F, Ansorge W, Draetta G. Cyclin A is required at two points in the human cell cycle. EMBO J. 1992;11:961–71. https://doi.org/10.1002/j.1460-2075.1992.tb05135.x.
29. Sebastian B, Kakizuka A, Hunter T. Cdc25m2 activation of cyclin-dependent kinases by dephosphorylation of Threonine-14 and Tyrosine-15. P Natl Acad Sci USA. 1993;90:3521–4. https://doi.org/10.1073/pnas.90.8.3521.
30. Hegarat N, Crncec A, Suarez Peredo Rodriguez MF, Echegaray Iturra F, Gu Y, Busby O, et al. Cyclin A triggers mitosis either via the Greatwall kinase pathway or cyclin B. EMBO J. 2020;39:e104419. https://doi.org/10.15252/embj.2020104419.
31. Yu J, Li S, Qi J, Chen Z, Wu Y, Guo J, et al. Cleavage of GSDME by caspase-3 determines lobaplatin-induced pyroptosis in colon cancer cells. Cell Death Dis. 2019;10:193. https://doi.org/10.1038/s41419-019-1441-4.
32. Rogers C, Fernandes-Alnemri T, Mayes L, Alnemri D, Cingolani G, Alnemri ES. Cleavage of DFNA5 by caspase-3 during apoptosis mediates progression to secondary necrotic/pyroptotic cell death. Nat Commun. 2017;8:14128. https://doi.org/10.1038/ncomms14128.
33. Hu L, Chen M, Chen XR, Zhao CG, Fang ZY, Wang HZ, et al. Chemotherapy-induced pyroptosis is mediated by BAK/BAX-caspase-3-GSDME pathway and inhibited by 2-bromopalmitate. Cell Death Dis. 2020;11:281. https://doi.org/10.1038/s41419-020-2476-2.
34. Wang YP, Gao WQ, Shi XY, Ding JJ, Liu W, He HB, et al. Chemotherapy drugs induce pyroptosis through caspase-3 cleavage of a gasdermin. Nature. 2017;547:99–103. https://doi.org/10.1038/nature22393.
35. An H, Heo JS, Kim P, Lian Z, Lee S, Park J, et al. Tetraarsenic hexoxide enhances generation of mitochondrial ROS to promote pyroptosis by inducing the activation of caspase-3/GSDME in triple-negative breast cancer cells. Cell Death Dis. 2021;12:159. https://doi.org/10.1038/s41419-021-03454-9.
36. Xu WF, Che Y, Zhang Q, Huang H, Ding CJ, Wang Y, et al. Apaf-1 pyroptosome senses mitochondrial permeability transition. Cell Metab. 2021;33:424–36. https://doi.org/10.1016/j.cmet.2020.11.018.
37. Bertheloot D, Latz E, Franklin BS. Necroptosis, pyroptosis and apoptosis: an intricate game of cell death. Cell Mol Immunol. 2021;18:1106–21. https://doi.org/10.1038/s41423-020-00630-3.
38. Newton K, Strasser A, Kayagaki N, Dixit VM. Cell death. Cell. 2024;187:235–56. https://doi.org/10.1016/j.cell.2023.11.044.

39. Gao J, Xiong A, Liu J, Li X, Wang J, Zhang L, et al. PANoptosis: bridging apoptosis, pyroptosis, and necroptosis in cancer progression and treatment. Cancer Gene Ther. 2024;31:970–83. https://doi.org/10.1038/s41417-024-00765-9.
40. Samir P, Malireddi RKS, Kanneganti TD. The PANoptosome: a deadly protein complex driving pyroptosis, apoptosis, and necroptosis (PANoptosis). Front Cell Infect Microbiol. 2020;10:238. https://doi.org/10.3389/fcimb.2020.00238.
41. Fritsch M, Gunther SD, Schwarzer R, Albert MC, Schorn F, Werthenbach JP, et al. Caspase-8 is the molecular switch for apoptosis, necroptosis and pyroptosis. Nature. 2019;575:683–7. https://doi.org/10.1038/s41586-019-1770-6.
42. Schwarzer R, Jiao H, Wachsmuth L, Tresch A, Pasparakis M. FADD and Caspase-8 regulate gut homeostasis and inflammation by Controlling MLKL- and GSDMD-Mediated death of intestinal epithelial cells. Immunity. 2020;52:978–e993976. https://doi.org/10.1016/j.immuni.2020.04.002.
43. Dowsett M, Dunbier AK. Emerging biomarkers and new understanding of traditional markers in personalized therapy for breast cancer. Clin Cancer Res. 2008;14:8019–26. https://doi.org/10.1158/1078-0432.CCR-08-0974.
44. Saiwaki T, Kotera I, Sasaki M, Takagi M, Yoneda Y. In vivo dynamics and kinetics of pKi-67: transition from a mobile to an immobile form at the onset of anaphase. Exp Cell Res. 2005;308:123–34. https://doi.org/10.1016/j.yexcr.2005.04.010.
45. Miller I, Min M, Yang C, Tian C, Gookin S, Carter D, et al. Ki67 is a graded rather than a binary marker of Proliferation versus Quiescence. Cell Rep. 2018;24:1105–e11121105. https://doi.org/10.1016/j.celrep.2018.06.110.
46. Geng Y, Yu Q, Whoriskey W, Dick F, Tsai KY, Ford HL, et al. Expression of cyclins E1 and E2 during mouse development and in neoplasia. Proc Natl Acad Sci U S A. 2001;98:13138–43. https://doi.org/10.1073/pnas.231487798.
47. Chu C, Geng Y, Zhou Y, Sicinski P. Cyclin E in normal physiology and disease states. Trends Cell Biol. 2021;31:732–46. https://doi.org/10.1016/j.tcb.2021.05.001.
48. Honda R, Lowe ED, Dubinina E, Skamnaki V, Cook A, Brown NR, et al. The structure of cyclin E1/CDK2: implications for CDK2 activation and CDK2-independent roles. EMBO J. 2005;24:452–63. https://doi.org/10.1038/sj.emboj.7600554.
49. Kok YP, Guerrero Llobet S, Schoonen PM, Everts M, Bhattacharya A, Fehrmann RSN, et al. Overexpression of cyclin E1 or Cdc25A leads to replication stress, mitotic aberrancies, and increased sensitivity to replication checkpoint inhibitors. Oncogenesis. 2020;9:88. https://doi.org/10.1038/s41389-020-00270-2.
50. Zeng J, Hills SA, Ozono E, Diffley JFX. Cyclin E-induced replicative stress drives p53-dependent whole-genome duplication. Cell. 2023;186:528–e542514. https://doi.org/10.1016/j.cell.2022.12.036.
51. Chaudhuri AR, Nussenzweig A. The multifaceted roles of PARP1 in DNA repair and chromatin remodelling. Nat Rev Mol Cell Bio. 2017;18:610–21. https://doi.org/10.1038/nrm.2017.53.
52. Fu HY, Liu RD, Jia ZX, Li R, Zhu FF, Zhu WX, et al. Poly(ADP-ribosylation) of P-TEFb by PARP1 disrupts phase separation to inhibit global transcription after DNA damage. Nat Cell Biol. 2022;24:513–25. https://doi.org/10.1038/s41556-022-00872-5.
53. Chen Q, Ma K, Liu XH, Chen SH, Li P, Yu YH, et al. Truncated PARP1 mediates ADP-ribosylation of RNA polymerase III for apoptosis. Cell Discov. 2022;8:3. https://doi.org/10.1038/s41421-021-00355-1.
54. Mashimo M, Onishi M, Uno A, Tanimichi A, Nobeyama A, Mori M, et al. The 89-kDa PARP1 cleavage fragment serves as a cytoplasmic PAR carrier to induce AIF-mediated apoptosis. J Biol Chem. 2021;296:100046. https://doi.org/10.1074/jbc.RA120.014479.
55. Xu HB, Shen XM, Li XK, Yang XH, Chen C, Luo DQ. The natural product dehydrocurvularin induces apoptosis of gastric cancer cells by activating PARP-1 and caspase-3. Apoptosis. 2023;28:525–38. https://doi.org/10.1007/s10495-023-01811-x.
56. D'Amours D, Germain M, Orth K, Dixit VM, Poirier GG. Proteolysis of poly(ADP-ribose) polymerase by caspase 3: kinetics of cleavage of mono(ADP-ribosyl) ated and DNA-bound substrates. Radiat Res. 1998;150:3–10. https://doi.org/10.2307/3579638.

Publisher's Note